



# A Limit Equilibrium Model to Simulate the Large-Scale Pillar Collapse at the Everest Platinum Mine

P. M. Couto<sup>1</sup> · D. F. Malan<sup>1</sup>

Received: 20 May 2022 / Accepted: 20 September 2022 / Published online: 5 October 2022  
© The Author(s), under exclusive licence to Springer-Verlag GmbH Austria, part of Springer Nature 2022

## Abstract

This paper is a case study of a large-scale pillar collapse at the Everest Platinum Mine. A major contributing factor to the collapse was the presence of weak alteration layers in the pillars. These alteration layers are found in the Bushveld Complex in South Africa where the pyroxenite layers have been exposed to hydrothermal fluid flow, serpentinisation and layer-parallel shearing. The resulting clay-like material and the weak partings substantially reduce the pillar strength. From the literature survey, it is clear that weak seams in pillars reduce their strength and conventional pillar strength formulas overestimate the strength in these cases. As an alternative, a novel numerical modelling approach is proposed to study the pillar failure and to conduct a back analysis of the mine collapse. This consists of a limit equilibrium constitutive model implemented in a displacement discontinuity code. Two areas of the mine were simulated, namely part of the collapsed area and a second area, with larger pillars that is still stable. This allowed for a preliminary calibration of the limit equilibrium model. The model illustrated that a reduction in friction angle on the partings, owing to the presence of water in the collapse area, seems to be a factor that contributed to the collapse. Although encouraging results are obtained, calibration of the limit equilibrium model remains a challenge. Laboratory testing is required in future to determine the strengths of the weak partings and in particular, the difference in strength of the wet and dry alteration zone material.

## Highlights

- Geological alterations substantially reduce the strength of hard rock pillars and the classical approach of using empirical pillar strength formulae for layout design does not work in these cases.
- A novel approach to simulate the pillar failure on a mine-wide scale is presented in this paper and this consists of a displacement discontinuity boundary element method using a limit equilibrium model to represent the pillar failure.
- The collapse of the Everest Platinum Mine in South Africa is described in the paper, it is used to test the proposed methodology, and it provides valuable data for researchers interested in case studies where pillar strength is reduced by weak layers.
- The proposed modelling methodology seems valuable to simulate the pillar failure and to design layouts for these types of ground conditions. Calibration of the limit equilibrium model remains a challenge, however.

**Keywords** Pillar failure · Weak seam · Limit equilibrium model · Bord and pillar layout

## 1 Introduction

An overview of the important aspects of hard rock pillar design is given by a number of authors (see, e.g. Lunder and Pakalnis 1997; Martin and Maybee 2000; Gonzalez-Nicieza et al. 2006; Esterhuizen et al. 2011). The pillar strength and stress distribution in the proposed layout is required to design a stable excavation. As a complicating factor, weak

✉ D. F. Malan  
francois.malan@up.ac.za

<sup>1</sup> Department of Mining Engineering, University of Pretoria, Pretoria, South Africa

layers in the pillars reduce the pillar strength and these layers can cause large-scale collapses (Malan and Napier 2011). Esterhuizen and Ellenberger (2007) studied the effects of weak layers on pillar stability in stone mines in the USA. This study was prompted by observations of weak bands in the pillars causing failure at unexpectedly low stresses. It appeared that extrusion of the weak layers contributed to the failure of the pillars. FLAC2D numerical modelling was done to study the mechanism of failure. The properties of the weak layers were simply selected from the database of properties in FLAC and were similar to those of a “clayey soil”. This highlights a difficulty of these weak-layer pillar problems as it is difficult to obtain representative samples of the layers for laboratory testing. The modelling confirmed the hypothesis that the extrusion of the failed weak material results in tensile stresses in the stronger rock, thereby facilitating failure at lower stress levels. The authors found that the strength reduction of the pillar is a function of the compressive strength of the weak layers, the frictional properties and the thickness of these bands. Furthermore, a single weak band, except if it comprises more than two percent of the pillar height, does not affect pillars as severely as multiple bands. The modelling indicated that slender pillars are affected to a greater extent by the presence of weak bands compared to wider pillars.

In the South African platinum mines, weak partings with infilling are also referred to as “alteration layers”. In contrast to the angular discontinuities described by Esterhuizen et al. (2019), these alteration layers are typically sub-parallel to the dip of the reef and, therefore, normal to the axis of the

pillars. Hartzenberg et al. (2019) defines alteration layers as follows: “The hangingwall contact of the UG2 Chromitite Reef at these sites consists of pyroxenite. The pyroxenite layers have been exposed to hydrothermal fluid flow, serpentinisation and layer-parallel shearing. The resulting clay-like material (weak partings) is defined as the alteration zone”. The term “alteration layers” are also adopted in this paper for the partings with the weak infilling. Figure 1 illustrates this alteration zone at the contact between the pillar and the hanging wall at the Everest Platinum Mine. Note the varying thickness of the layer. Almost no research has been done on the effect of this layer on pillar strength. The low friction angle between the layer and the host rock, as well as the low strength of the alteration layer, seems to reduce the pillar strength substantially and the resulting typical pillar failure is shown in Fig. 2.

From the discussion above, it is clear that a revised pillar design methodology is required in areas where the alteration zone is present. Ideally, a careful back analysis of failed pillar layouts, if available, will be required to determine actual pillar strengths. The pillar strengths estimated from these studies will enable the simulation of future extraction sequences and optimal pillar sizes and the spacing of barrier pillars can be selected. As illustrated in this paper, the pillar shapes are mostly irregular in the tabular hard rock bord and pillar mines and the displacement discontinuity boundary element method is, therefore, the preferred method for this back analysis. A number of workers illustrated that this approach provides a useful representation of tabular mine layouts (Plewman et al. 1969; Deist et al. 1972; Crouch

**Fig. 1** A weak alteration layer is present at the contact between the pillar and the hanging wall at the Everest Platinum Mine

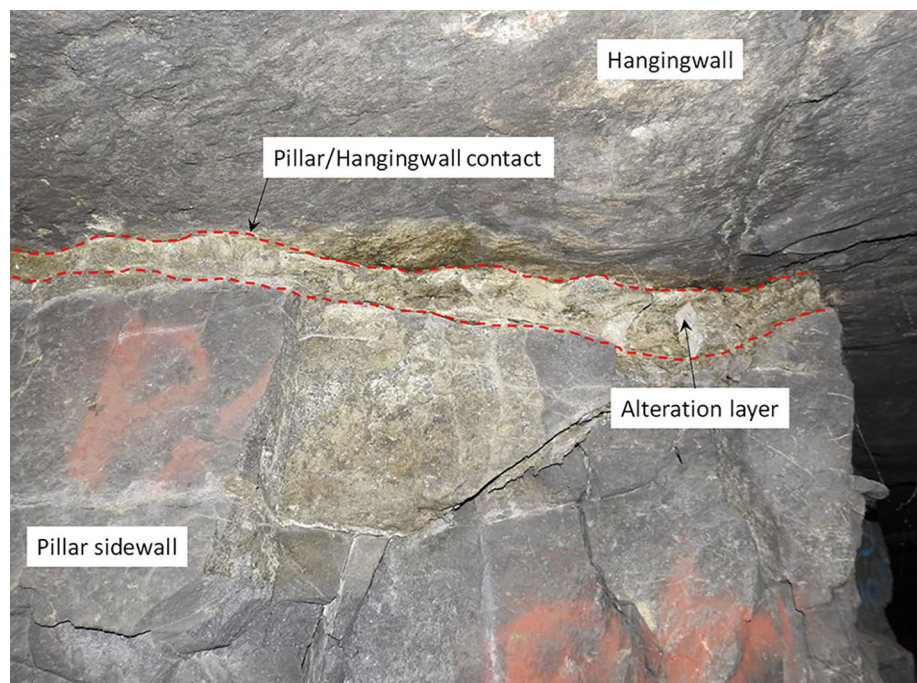
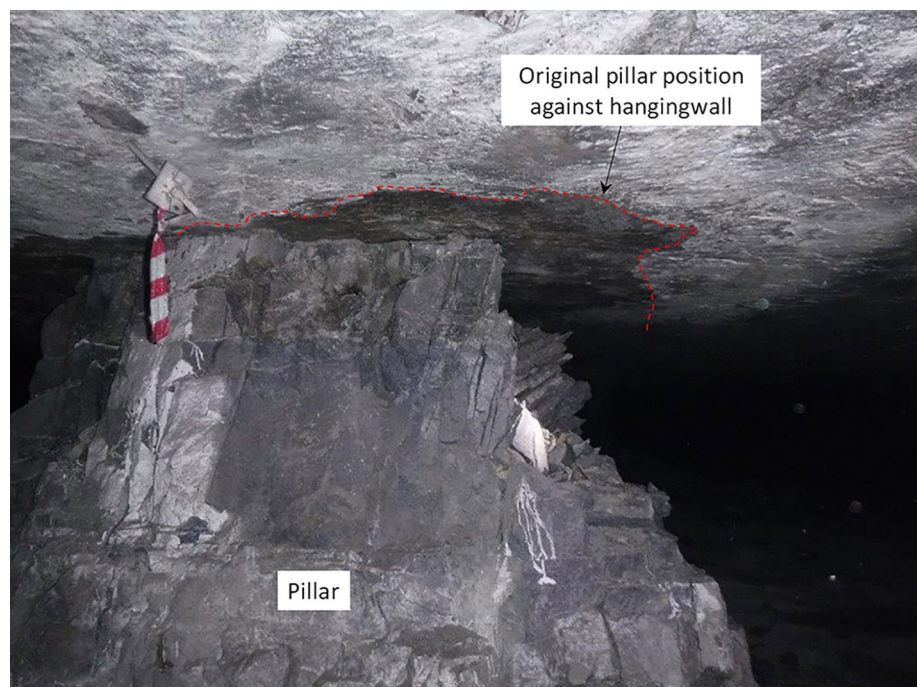


**Fig. 2** Typical pillar failure in areas where weak alteration zones are present. Note the original size of the pillar against the hanging wall as indicated by the red dotted line (colour figure online)



and Starfield 1983; Salamon 1964; Ryder and Napier 1985; Heasley 1998). An unstructured triangular element mesh is used in this study to represent the irregular pillar shapes. A drawback of this technique is that the excavation stress distribution in the normal direction to the mining horizon near the excavation edges is not an accurate reflection of the actual stress. This difficulty is addressed in the paper using a limit equilibrium model of the edge failure zone. This seemed to be a useful approach to simulate the pillar failure induced by the weak alteration zone. The collapse of the Everest Platinum Mine in South Africa is described in the paper and it is used as a case study to test the proposed modelling methodology. The difficulty of calibrating the model, especially in the absence of a good mine collapse case study and laboratory testing data, is a drawback and is discussed. This will nevertheless also be the case for any other inelastic modelling approach.

## 2 The Collapse of the Everest Platinum Mine

The Everest Platinum Mine is located in the Eastern Bushveld Complex of South Africa near the town of Lydenburg. The Bushveld Complex is the world's largest layered igneous intrusion and it hosts the world's single largest deposit of platinum group metals. The Complex consists of a 7–9 km thick sequence of mafic to ultramafic cyclic units. The mafic rocks are known as the Rustenburg Layered Suite that sub-outcrop around the periphery of the complex and dip towards its centre. The Rustenburg Layered Suite

is subdivided into five zones, of which the Critical Zone is the most important as it contains the economically important horizons that contain the platinum group metals and the chromitite seams (e.g. see Roberts and Clark-Mostert 2010; Eriksson et al. 1995). Figure 3 illustrates one of the chrome seams as exposed above the entrance of a chrome mine in the Eastern Bushveld Complex. Note the tabular nature of the seam and it dips at shallow angle ( $\approx 9^\circ$ ) into the page. The two mineralised layers, which contain the economically important platinum group metals, are the Merensky reef and the Upper Group 2 (UG2) chromitite layer. Only the UG2 reef was mined at Everest Platinum Mine.

At Everest Platinum Mine, a reef parallel alteration zone undulates close to the top reef contact. The material of the alteration zone is weathered, clay-like and moist close to surface, but more competent and solid at greater depths. The appearance of this zone at the deeper levels has been shown in Fig. 1. The nature of this material when it is wet and subjected to shear is shown in Fig. 4.

The pillar design at Everest Platinum Mine was originally done using the empirical strength equation developed by Hedley and Grant (1972) and modified by Stacey and Page (1986). Similar to standard industry practice, a factor of safety of 1.5 was adopted. For the UG2 pillar design, the  $K$  value at Everest Platinum Mine was estimated to be 35 MPa.

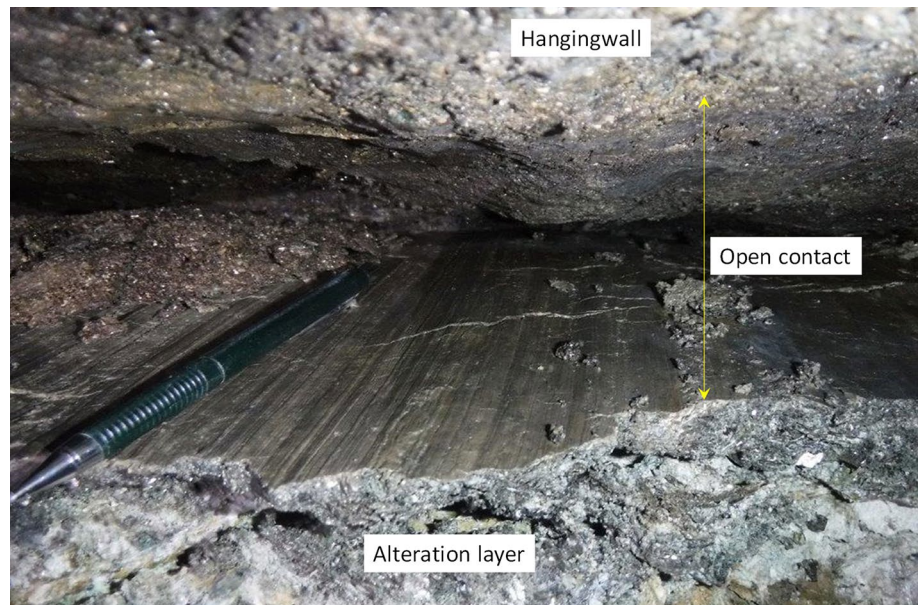
In terms of the sequence of events, during 2007, spalling of some of the pillars in the shallow sections of the mine were observed. As a result, the mine implemented an increase in pillar sizes and the decline pillars were supported using shotcrete. Closure instrumentation was installed and



**Fig. 3** A black chromitite seam visible above the portal of a chrome mine in the Bushveld Complex



**Fig. 4** The clay-like nature of the alteration layer in the shallower sections of the mine. Note the evidence of shear movement on this contact



by November 2008, these instruments recorded 5 mm of closure in the unstable area. On 23 November 2008, 220 mm of rain fell in one day and this contributed to the instability. The water pumps in the surface mine were inundated and excessive water seepage along the alteration zone occurred. It is hypothesized that this water became a significant contributing factor to the large collapse that occurred soon afterwards on 8 December 2008. The mine is relatively shallow and the collapse resulted in subsidence being recorded on surface. The extent of the collapse is shown in Fig. 5.

The authors recently conducted underground visits to record the current condition of the failed pillars (Figs. 6 and 7). No mining has been done at Everest Platinum Mine for approximately 11 years and only the essential services under the care and maintenance strategy have continued. These are limited to the pumping of water and the inspections of escape ways. Unfortunately, the inflow of water was never measured or assessed and the role of water in the possible ongoing deterioration of the pillars cannot be quantified. The initial pillar design, in the area where the



**Fig. 5** Mining outline of Everest Platinum Mine during December 2008 and the extent of the collapse. The coloured pillars indicate the different levels of damage of the pillars (colour figure online)

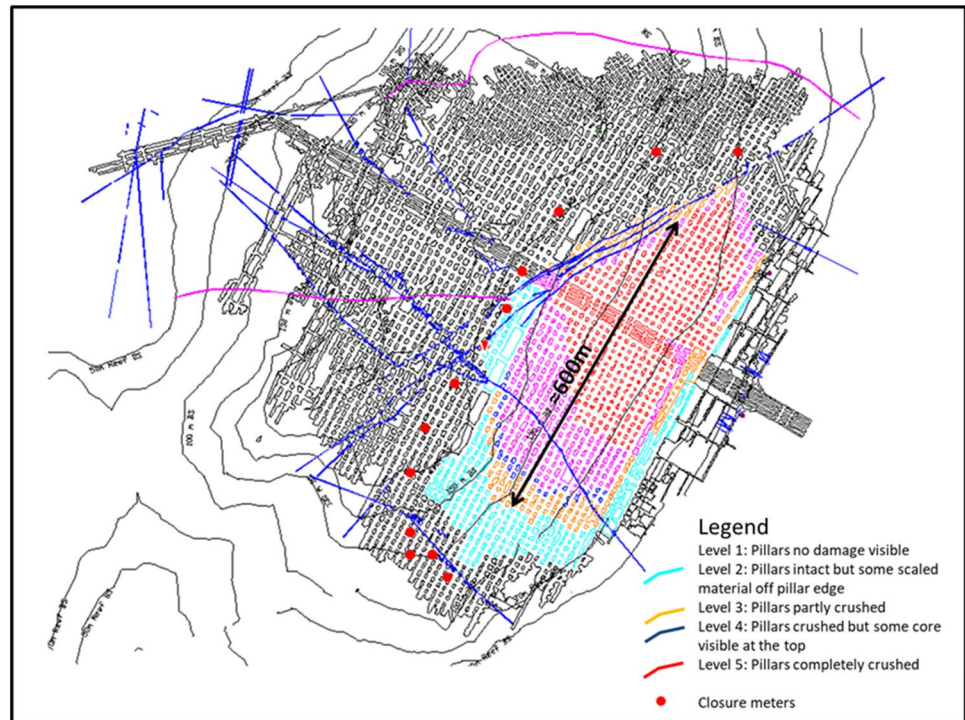
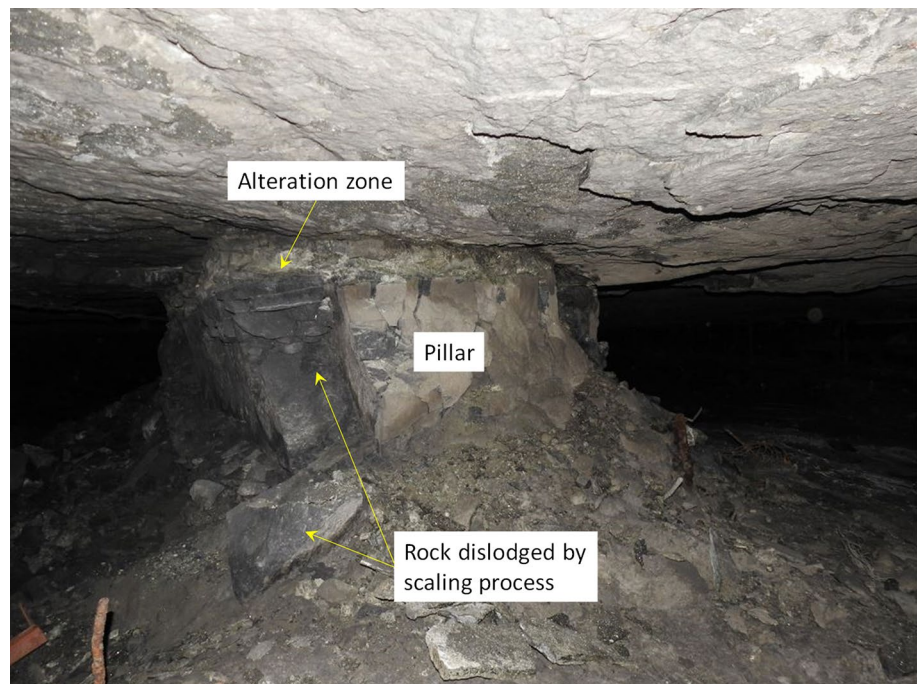


**Fig. 6** Extensive spalling of a pillar in the level 3 failure zone



collapse occurred, resulted in pillar dimensions ranging from  $5 \times 5$  to  $6 \times 6$  m, depending on depth. It is important to note that many of the pillars that could be measured during the underground visits were smaller than these sizes. The mining plan based on survey offsets done prior to 2008 also indicated that the pillar cutting was done poorly.

Many pillars were cut smaller than the design specifications and this is considered an important contributing factor to the collapse. The depth of pillar spalling could be estimated during the underground visits as the original boundaries of many of the pillars were still visible on the hanging wall as a result of the colour contrasts. As an

**Fig. 7** The pillars adjacent to the decline at Everest Platinum Mine were completely crushed during the collapse



example, the original pillar size can be seen on the hanging wall in Fig. 2.

The stoping width was measured at a number of points during the underground visits. Historical records indicate that the mining height varied between 2 and 2.2 m. Measurements of the stoping height, in the zone where no pillar failure was observed, gave an average value of 2.1 m. Closer to the declines, the stoping width gradually decreased, with a final stoping width of 1.3 m in the decline area. The amount of convergence was, therefore, approximately 0.7 m. Tensile cracks, with an open width of up to 1 cm, was observed close to the declines.

The weathering of the alteration zone in the pillars was evident. The presence of water and high humidity have allowed the alteration to deteriorate into a “muddy” composition that appears to have no cohesive properties and a low friction angle. This material needs to be tested in future to quantify the strength and friction angle. For the purposes of this study, the friction angles were estimated as discussed below. In many areas, the alteration zone “squeezed” out between the reef contact and the hanging wall contact. This has also resulted in slickenside surfaces clearly visible on the up-dip side of the pillars (Fig. 4).

In summary, the pillar rehabilitation measures implemented by the mine was not successful in the shallow areas. Figure 8 illustrates the cracking of the shotcrete applied to some of the pillars. From the literature (e.g. Alejano et al. 2017), it seems as if pillar support can be beneficial in some cases, but it did not work at Everest Platinum Mine. Many questions also remain with regards to the actual pillar

strength and if an alternative layout should have been implemented. The section below describes a modelling approach to obtain additional information about the pillar strength and layout stability.

### 3 Characteristics of the Limit Equilibrium Model Implemented in the Displacement Discontinuity Code TEXAN

To simulate the mine collapse shown above, a novel approach of using a limit equilibrium constitutive model in the displacement discontinuity boundary element code, TEXAN, was explored. The TEXAN code was originally developed to simulate the shallow bord and pillar layouts in the platinum industry in South Africa (Napier and Malan 2007). The code can solve two-dimensional and three-dimensional problems with multiple tabular reef planes at arbitrary orientations. Planar fault planes can also be included. These planes are tessellated with elements to represent ride and elastic convergence in stopes or to simulate slip on fault planes. The elements can be in an “infinite” space or in a “semi-infinite” space with a flat, stress-free surface. The host rock is assumed to be an isotropic elastic medium. Each element can have one or more collocation points giving constant or higher order variation discontinuity densities. Triangular elements can be defined to have one, ten or fifteen internal collocation points giving constant, cubic or quartic discontinuity variations, respectively. Quadrilateral elements can also be defined.



**Fig. 8** Example of a failed attempt to rehabilitate a pillar using shotcrete

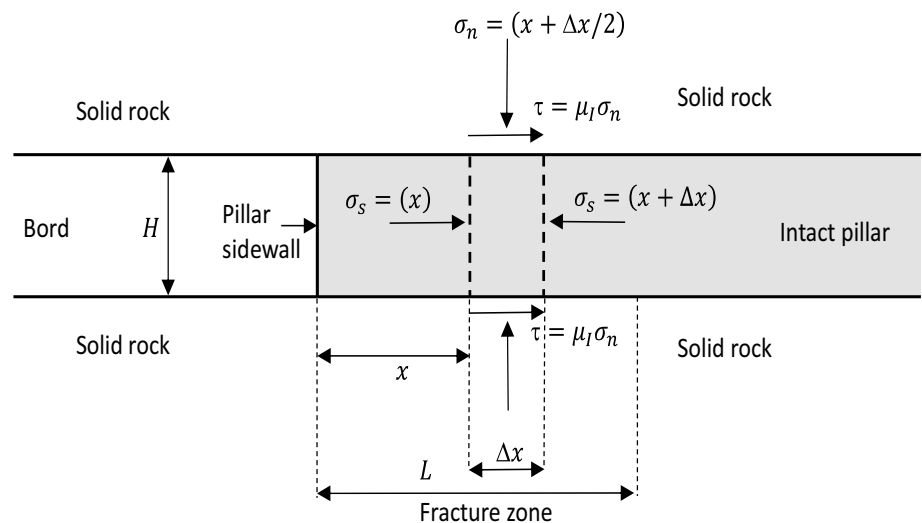


The motivation for using this modelling approach is that a large area had to be simulated to accurately compute the stresses acting on the pillars. The pillar cutting is often poor in the hard rock bord and pillar mines and a range of pillar sizes and shapes can be found. These complex geometries, with a large number of irregular-sized pillars, are difficult to build in finite difference or finite element codes. In contrast, displacement discontinuities boundary element models can easily overcome this problem. As a drawback, however, it is typically impossible for these displacement discontinuity codes to simulate the failure of the pillars. This problem can be circumvented using a limit equilibrium model and

this model is described in the paper. The characteristics and application of the limit equilibrium model have been explored in a number of studies (e.g. see Du Plessis et al. 2011; Napier and Malan 2018, 2021). The derivation of a simplified version of the model is given below to explore its applicability to the mechanism of pillar failure at Everest Platinum Mine.

Consider the force equilibrium of a slice of rock in the pillar shown in Fig. 9. This diagram illustrates the mined bord on the left and part of the pillar on the right. This simplistic model assumes the presence of an interface for the pillar contacts at both the hanging wall and footwall.

**Fig. 9** Force equilibrium of a slice of rock in a pillar



Typically, the edge of the pillar will fail where the stress exceeds the specified strength and the remainder of the pillar will remain intact. For weak material properties and high stress, the entire pillar can fail.

It is assumed that at  $x = 0$ , the edge of the pillar, the material is unconfined and that the seam-parallel stress component  $\sigma_s$  increases as  $x$  increases. The slice of rock indicated by the dotted lines in Fig. 9 is assumed to be in equilibrium. For this to be true, it is required that

$$H\sigma_s(x) + 2\tau\Delta x = H\sigma_s(x + \Delta x). \tag{1}$$

Note that the second term on the left of this equation reflects the effect of the interfaces at the hanging wall and footwall contacts. Equation (1) can be rearranged to give

$$\frac{\sigma_s(x + \Delta x) - \sigma_s(x)}{\Delta x} = \frac{2\tau}{H}. \tag{2}$$

The left-hand side of Eq. (2) is the definition of a derivative if  $\Delta x \rightarrow 0$  and, therefore, Eq. (2) can be written in the form of a differential equation if the width of the slice tends to zero:

$$\lim_{\Delta x \rightarrow 0} \frac{\sigma_s(x + \Delta x) - \sigma_s(x)}{\Delta x} = \frac{2\tau}{H} \tag{3}$$

or

$$\frac{d\sigma_s}{dx} = \frac{2\tau}{H}. \tag{4}$$

Equation (4) can only be solved if there is a relationship between  $\tau$  and  $\sigma_s$ . This is achieved by making the following two assumptions:

- (1) Assume that there is friction on the interfaces between the pillar, hanging wall and footwall, therefore,  $\tau$  is related to the pillar-normal stress  $\sigma_n$  by the following frictional slip condition:

$$\tau = \mu_l \sigma_n \tag{5}$$

where  $\mu_l$  is the coefficient of friction coefficient at the interface of the pillar contacts. Equation (5) can, therefore, also be written as

$$\tau = \tan \phi (\sigma_n) \tag{6}$$

where  $\phi$  is the friction angle on the interface.

- (2) Assume that  $\sigma_n$  is related to the seam-parallel stress component  $\sigma_s$  by a failure relationship of the form:

$$\sigma_n = m\sigma_s + \sigma_c \tag{7}$$

where  $\sigma_c$  and  $m$  are specified constants. Once failure occur,  $\sigma_c$  can be considered as the strength of the failed pillar material and  $m$  is a slope parameter. This slope

parameter simulates the confinement effect of the failed material on the edges of the pillar. A higher normal stress can, therefore, be found further away from the edge of the pillar.

Substituting Eqs. (6) and (7) into Eq. (4) gives the following differential equation:

$$\frac{d\sigma_s}{dx} = \frac{2 \tan \phi}{H} (m\sigma_s + \sigma_c). \tag{8}$$

Equation (8) can be integrated if the variables are separated as follows:

$$\int \frac{d\sigma_s}{m\sigma_s + \sigma_c} = \int \frac{2 \tan \phi}{H} dx. \tag{9}$$

The indefinite integral of the left-hand side of Eq. (9) can be solved as

$$\int \frac{d\sigma_s}{m\sigma_s + \sigma_c} = \frac{\ln(m\sigma_s + \sigma_c)}{m}. \tag{10}$$

This solution can be inserted into Eq. (9) and by solving the simple integral on the right side of Eq. (9), the following solution can be obtained. The solution depends on integration constant  $A$ :

$$\frac{\ln(m\sigma_s + \sigma_c)}{m} = \frac{2 \tan \phi x}{H} + A. \tag{11}$$

The constant  $A$  is derived by applying the boundary condition  $\sigma_s = 0$  when  $x = 0$ . This gives the value of  $A$  as

$$A = \frac{\ln(\sigma_c)}{m}. \tag{12}$$

Equation (12) can be inserted into (11) to give

$$\frac{\ln(m\sigma_s + \sigma_c)}{m} = \frac{2 \tan \phi x}{H} + \frac{\ln(\sigma_c)}{m} \tag{13}$$

and by combining the logarithmic expressions

$$\frac{1}{m} \ln \left( \frac{m\sigma_s + \sigma_c}{\sigma_c} \right) = \frac{2 \tan \phi x}{H}. \tag{14}$$

This can be written as

$$\frac{m\sigma_s + \sigma_c}{\sigma_c} = e^{2 \tan \phi mx/H} \tag{15}$$

and from this the solution of the seam-parallel stress follows as

$$\sigma_s = \frac{\sigma_c}{m} (e^{2 \tan \phi mx/H} - 1) \tag{16}$$



Equation (16) is written in a simpler form by assuming

$$\alpha = \frac{2 \tan \phi m}{H} \tag{17}$$

This gives

$$\sigma_s = \frac{\sigma_c}{m} (e^{\alpha x} - 1) \tag{18}$$

Substituting Eq. (18) into Eq. (7) gives an expression for  $\sigma_n$ :

$$\sigma_n = \sigma_c e^{\alpha x} \tag{19}$$

Equation (19) implies that the normal stress in the failed pillar edge increases exponentially from the edge towards the boundary between the failed and intact rock. This exponential increase in stress is characteristic of the model and it is not clear if this is an appropriate representation of the stress in a failed pillar. Also, important to consider is that it is a requirement that  $\sigma_c > 0$ , even after failure, otherwise the normal stress will be zero in all the failed parts of the pillar.

With regards to the weak interface at Everest Platinum Mine, from Eqs. (17) and (19), it is clear that the friction angle on the partings with the hanging wall and footwall play a prominent role in the subsequent distribution of stress in the pillar once failure initiates. Figure 10 illustrates the increase in stress from the edge of a failed pillar for different friction angles when assuming the parameters  $m = 2$ ,  $\sigma_c = 1$  MPa and  $H = 2$  m. The model is clearly sensitive to the selection of friction angle and the residual strength of the failed pillar rapidly decreases for low friction angles. Also

clear from the diagram is the very high stresses predicted in the centre of the pillar for large values of friction angles and higher values of  $m$ . These sharp peaks of stress in the centre of a failed pillar for high friction angles and slope parameter values are not considered realistic and is one of the drawbacks of the model.

The equations above are a simple derivation to illustrate the behaviour of the model. In the TEXAN code, a more complex model is implemented where there is a failure relationship between  $\sigma_n$  and  $\sigma_s$  for the intact pillar material given by

$$\sigma_n = m^i \sigma_s + \sigma_c^i \tag{20}$$

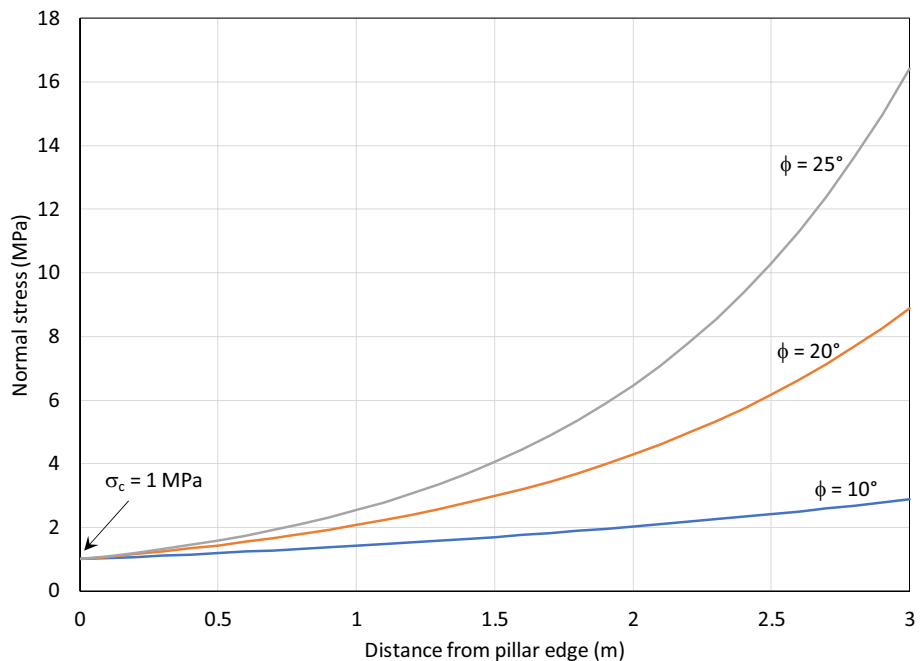
as well as for the failed pillar material

$$\sigma_n = m^f \sigma_s + \sigma_c^f \tag{21}$$

When specifying these parameters, the requirements of  $m^i \geq m^f$  and  $\sigma_c^i \geq \sigma_c^f$  must be met. As an illustration of the simulated model behaviour, a simple square pillar of 10 m width in the centre of a 50 × 50 m excavation was simulated (Fig. 11). The results illustrate the effect of the reducing the intact strength,  $\sigma_c^i$ , from 55 to 10 MPa while keeping the other parameters constant. For a value of 10 MPa, the pillar was completely crushed.

Also, important to note is that the TEXAN code assumes that the intact region of a pillar behaves according to a “spring” model that allows deformation in the normal direction. A “seam stiffness” value, therefore, also needs to be specified as an input parameter. Typically, this stiffness parameter is selected to match the deformation modulus of

**Fig. 10** Increase in normal stress acting on a completely failed pillar when assuming a limit equilibrium model. The pillar is 6 m wide and the centre of the pillar is at 3 m. The graph is plotted using parameters  $m = 2$ ,  $\sigma_c = 1$  MPa and  $H = 2$  m



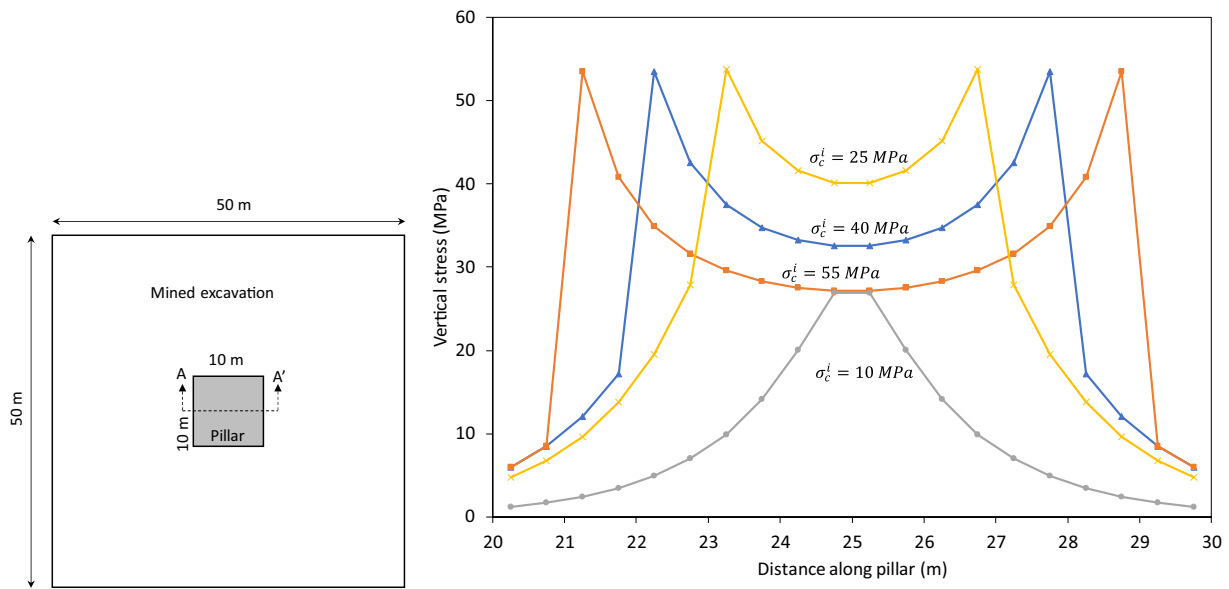


**Fig. 11** Simulated vertical stress along a 10 m wide pillar (section AA') for different values of  $\sigma_c^i$ . High values for this parameter result in a large intact core of the pillar and for low values, the pillar is com-

pletely crushed. The other parameters were  $m_i = m_f = 4$ ,  $\sigma_c^f = 4$  MPa,  $\phi = 10^\circ$  and  $H = 2$  m

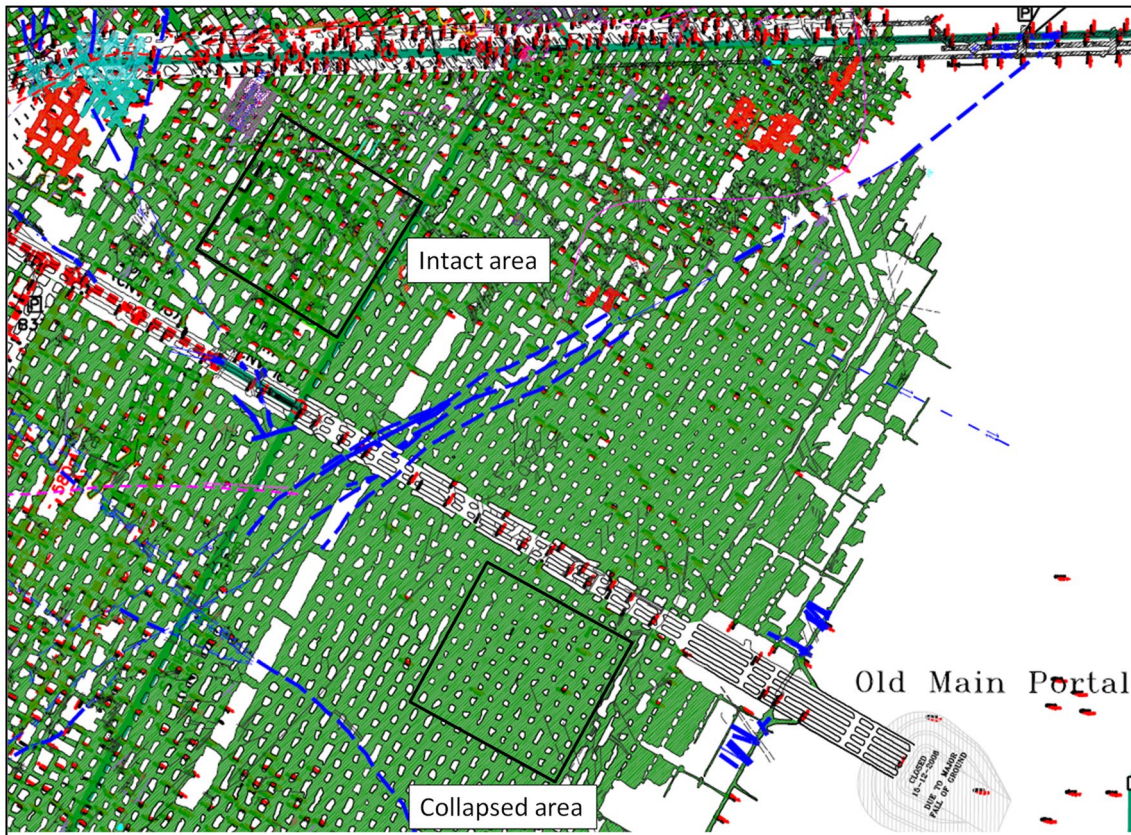


**Fig. 12** The two areas selected for detailed modelling (the two black squares) are shown in this figure. On these mine plans, the pillars are indicated by the white areas. Note that the pillar sizes are larger in the intact area



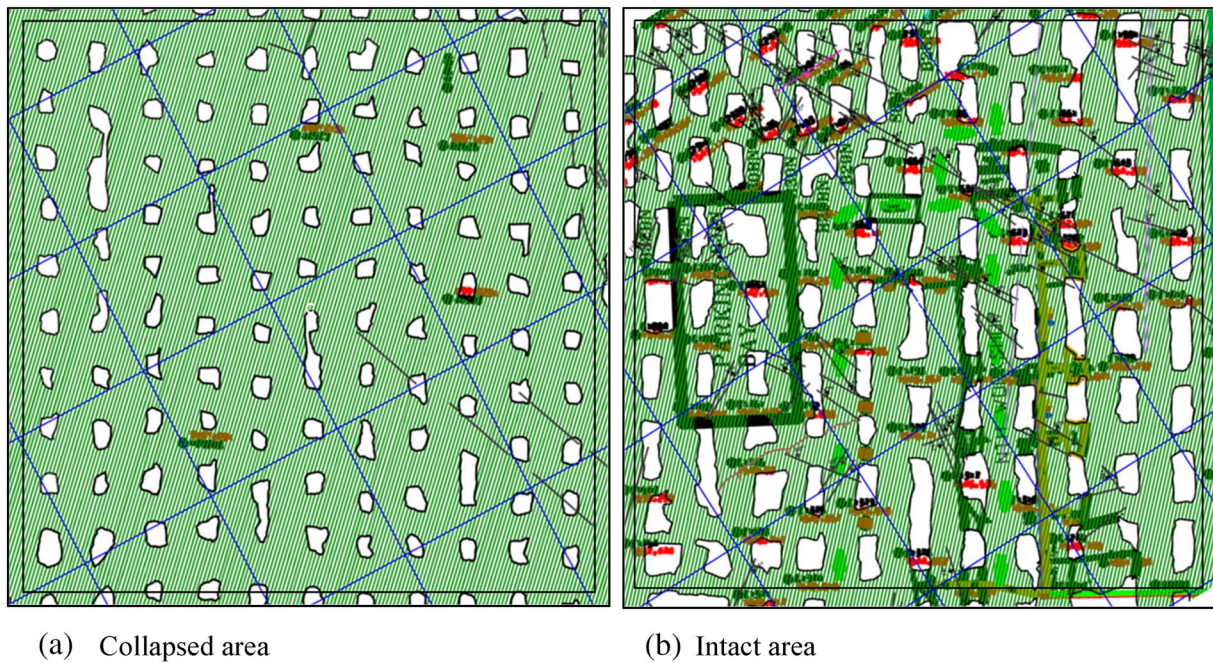


**Fig. 13** An enlarged view of the two areas selected for detailed modelling. Note the clear difference in pillar sizes. The extraction ratio of the collapsed area was 88% compared to the 67% of the intact

area. The sizes of both areas simulated were 160×160 m. The input parameters are given in Table 1. Again, note that on these mine plans the pillars are indicated by the white areas

**Table 1** Input parameters for the TEXAN modelling

Parameter	Value
Young's modulus	70 GPa
Poisson's ratio	0.2
Depth below surface, $h$	113 m (collapsed) and 217 m (intact)
Overburden density, $\rho$	3000 kg/m <sup>3</sup>
Intact strength, $\sigma_c^i$	25–60 MPa
Intact rock slope, $m^i$	4.6 and 7
Crushed rock strength $\sigma_c^f$	4–10 MPa
Crushed rock slope, $m^f$	4.6 and 7
Interface friction angle, $\phi$	5°–50°
Seam height, $H$	2.0 m
Seam stiffness modulus	35,000 MPa/m

Various parameters for the limit equilibrium model were tested to serve as a first-order calibration to match the underground observations

the host rock in the platinum industry. The code solves the normal stress acting on the pillar and test if failure of any of the elements will occur according to Eq. (20). If no failure occurs for a particular element, a small amount of strain will occur in the normal direction according to the stiffness parameter specified. If the particular element fails, new

strength parameters are adopted according to Eq. (21) and the excess stress for this element is redistributed to neighbouring elements. Very weak parameters and large numbers of failed pillars can result in a large number of iterations in the code, and increased solution times.

Furthermore, it is important to note that the description above is a simplified model to illustrate the concept. Napier and Malan (2021) gives additional detail of the implementation in a displacement discontinuity solution scheme using unstructured triangular elements to allow irregular plan-view pillar shapes and mining step increments to be represented. The seam-parallel confining stress distribution in the fracture zone is determined using a fast-marching solution algorithm.

The simplified derivation of the model is presented above to highlight another potential drawback of the approach. This assumes a symmetrical model with weak partings, with an identical friction angle, at both the hanging wall and footwall contacts of the pillar (see Fig. 9). The pillar failure at Everest Platinum Mine was caused by the alteration zone which is present only at the hanging wall contact (Fig. 1). The footwall contact is more competent and the friction angle for the footwall will be much higher. In the mine, this resulted in a “toppling” failure mechanism as shown in Fig. 2. The simplified limit equilibrium model cannot simulate this behaviour and a possible extension of the limit equilibrium model needs to be explored.



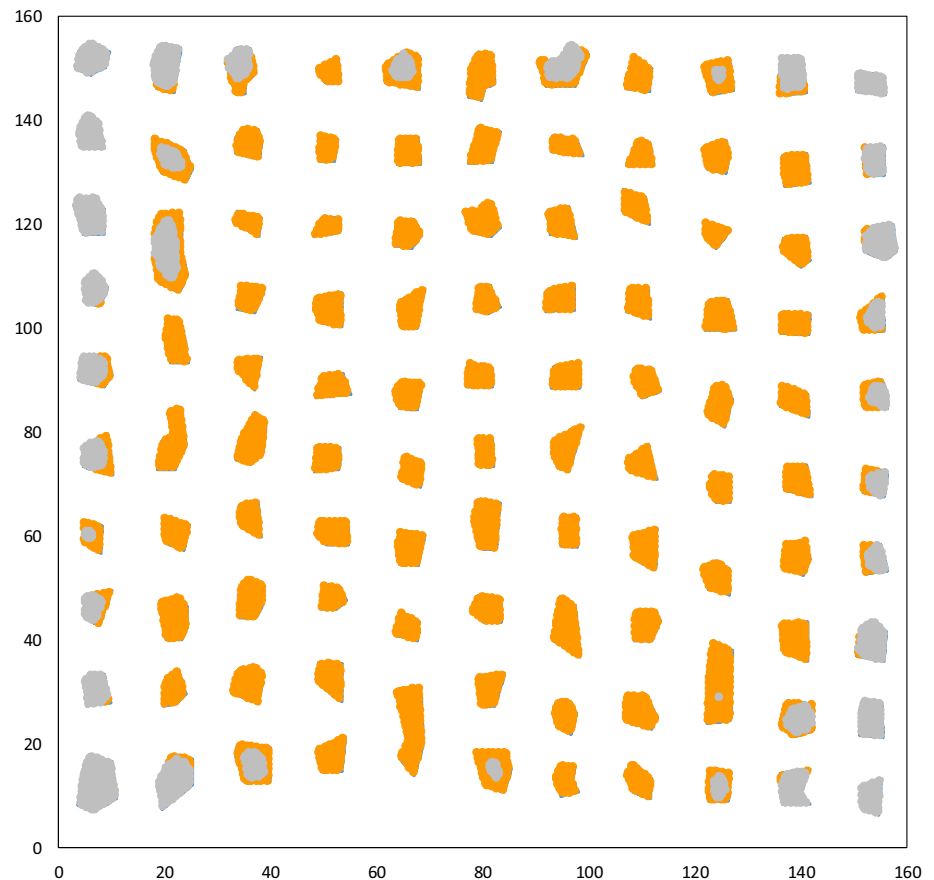
**Table 2** Model input parameters and pillar failure of the collapsed area for different parameter values

Parameters	Area 1: collapsed area															
	Set 1	Set 2	Set 3	Set 4	Set 5	Set 6	Set 7	Set 8	Set 9	Set 10	Set 11	Set 12	Set 13	Set 14	Set 15	Set 16
Intact strength (MPa)	60	25	30	30	30	30	30	30	30	30	30	30	30	30	30	30
Intact rock slope	7	4.6	4.6	4.6	4.6	4.6	4.6	4.6	4.6	4.6	4.6	4.6	4.6	4.6	4.6	4.6
Initial crush strength (MPa)	4	4	4	5	7.5	10	10	4	4	4	4	4	4	10	5	4
Crushed rock slope	7	4.6	4.6	4.6	4.6	4.6	4.6	4.6	4.6	4.6	4.6	4.6	4.6	4.6	4.6	4.6
Interface friction angle	30	10	20	20	20	20	20	20	20	25	15	10	5	15	15	10
Seam height (m)	2	2	2	2	2	2	2	2	2	2	2	2	2	2	2	2
Seam stiffness modulus (MPa/m)	45,000	45,000	45,000	45,000	45,000	45,000	45,000	45,000	45,000	45,000	45,000	45,000	45,000	45,000	45,000	45,000
Pillar failure percentage (%)	0.0	72.9	30.6	23.2	10.9	5.3	20.9	50.3	72.3	91.1	11.3	36.2	74.1			

**Table 3** Model input parameters and pillar failure of the intact area for different parameter values

Parameters	Area 2: intact area															
	Set 1	Set 2	Set 3	Set 4	Set 5	Set 6	Set 7	Set 8	Set 9	Set 10	Set 11	Set 12	Set 13	Set 14	Set 15	Set 16
Intact strength (MPa)	60	25	30	30	30	30	30	30	30	30	30	30	30	30	30	30
Intact rock slope	7	4.6	4.6	4.6	4.6	4.6	4.6	4.6	4.6	4.6	4.6	4.6	4.6	4.6	4.6	4.6
Initial crush strength (MPa)	4	4	4	4	4	4	5	7.5	10	4	4	4	4	10	5	4
Crushed rock slope	7	4.6	4.6	4.6	4.6	4.6	4.6	4.6	4.6	4.6	4.6	4.6	4.6	4.6	4.6	4.6
Interface friction angle	30	10	30	40	50	20	20	20	20	20	25	15	10	5	15	10
Seam height (m)	2	2	2	2	2	2	2	2	2	2	2	2	2	2	2	2
Seam stiffness modulus (MPa/m)	45,000	45,000	45,000	45,000	45,000	45,000	45,000	45,000	45,000	45,000	45,000	45,000	45,000	45,000	45,000	45,000
Pillar failure percentage (%)	0.0	81.9	13.7	6.2	2.2	26.4	21.3	14.0	8.7	18.8	43.8	80.8	99.5	4.8	34.3	82.3

**Fig. 14** Simulation of pillar failure for the collapsed area using the “Set 12” calibration parameters. The orange colour denotes failure and the grey denotes intact pillars (colour figure online)



#### 4 Back-Analysis of the Everest Platinum Mine Pillars

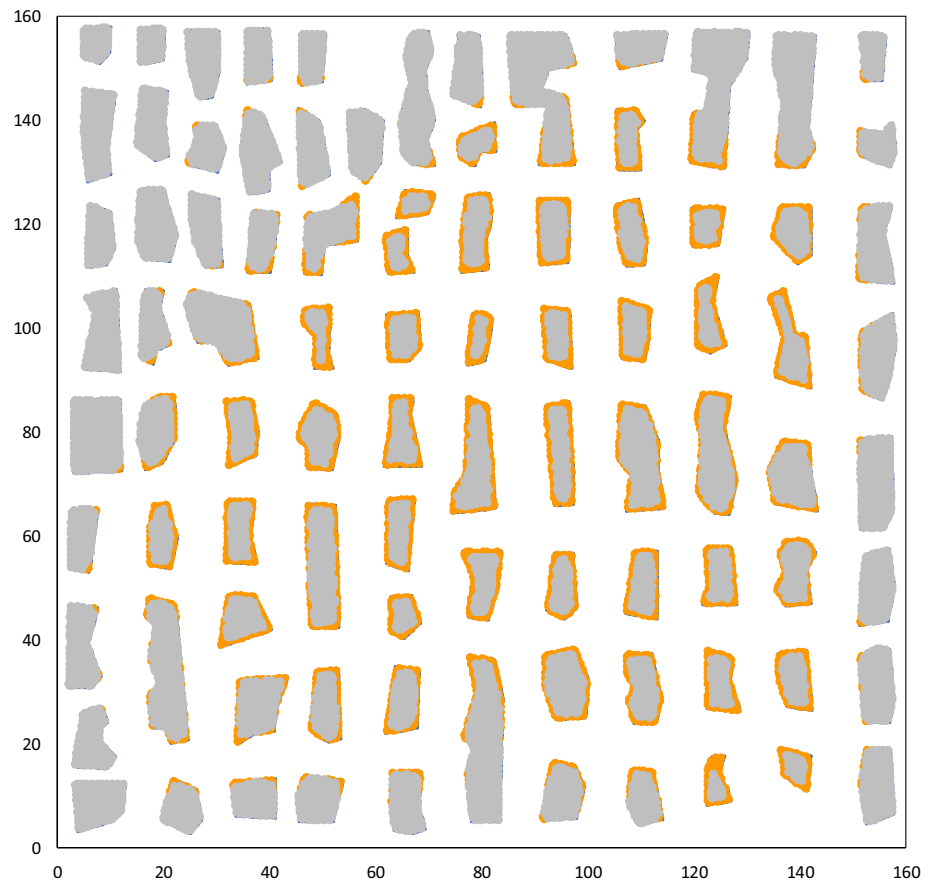
Figure 12 illustrates the two areas of the mine selected for modelling. These were selected based on the underground observations of total pillar collapse in the one area and mostly intact pillars in the other area. The sizes of the pillars in the two blocks clearly show the difference in the pillar sizes. The depth below surface for the two areas vary and they were modelled at the correct depth below surface. Ideally, larger areas should have been simulated, but small triangular element sizes had to be used for the limit equilibrium model and the TEXAN code was limited in terms of the number of elements it could solve during the time of this study.

Figure 13 illustrates enlarged views of the two areas. As the areas were simulated with no dip, they were also rotated to simplify the digitizing and meshing process for the models. The pillar shapes shown in Fig. 13 were approximated using straight line polygons. This simplified the digitizing and meshing process using triangular elements.

To select the most appropriate parameters, it had to be considered that the presence of water was a key difference between the intact area and the collapsed area. The alteration

zone was dry in the intact area and moist in the collapsed area. The friction angle of the pillar contact with the hanging wall was, therefore, probably lower in the collapsed area compared to the intact area. Unfortunately, no laboratory test results of these friction angles were available during the study and this needs to be explored in future. Wyllie and Norrish (1996) published data on the friction angles of discontinuities with clay infillings and values between  $8^\circ$  and  $20^\circ$  are presented. The effect of moisture may decrease this friction angle. For example, Deng et al. (2018) noted a decrease in soil friction angle from  $15.6^\circ$  to  $9.9^\circ$  if the moisture content increases from 19 to 30%. In the absence of laboratory data for the Everest Platinum Mine alteration zone, a number of numerical simulations were conducted with friction angles ranging from  $5^\circ$  to  $30^\circ$ . The different parameters are shown in Tables 2 and 3. Based on the various simulations and by comparing the pillar fracturing with the underground observations, the parameters of “Set 12” for the collapsed area (Table 2) and the parameters for “Set 10” for the intact area (Table 3) are considered to be the best initial calibration. The only difference between these two sets is the friction angle ( $10^\circ$  for the collapsed area and  $25^\circ$  for the intact area). This seems plausible as the other rock parameters are considered to be identical for both areas. It should be noted that this is only a first, and rather crude, attempt to

**Fig. 15** Simulation of pillar failure for the intact area using the “Set 10” calibration parameters. The orange colour denotes failure and the grey denotes intact pillars (colour figure online)



calibrate the parameters in the absence of laboratory testing data. It was nevertheless valuable to illustrate the value of this numerical model approach. In future, detailed laboratory experiments of the rock strengths and the alteration zone, as well as underground measurements of parameters such as pillar spalling depths, are required to improve upon this calibration.

The simulated condition of the pillars in the two areas are shown in Figs. 14 and 15. These are encouraging results as the pillars in the centre of the collapsed area are completely failed and there is only minor spalling in the centre of the intact area. This agrees with the underground observations for the two areas. The pillars on the edges of the collapsed area are still intact, but this is caused by the modelled abutment next to these pillars and the relatively small size of the model.

From these results, it seems as if the particular numerical model is able to simulate the observed pillar behaviour. Encouraging was that the same parameters could be used for the stable and intact area except that the friction angle of the interfaces were varied. A challenging aspect is that the calibration of the limit equilibrium model is very difficult. Future work needs to study methods to better calibrate this model. Laboratory testing is required to determine the rock strengths as well as the friction angles of the wet and dry

alteration zone material. As the proposed model seems capable to simulate the behaviour of the pillars, this model can be used to investigate an alternative layout that will ensure stable excavations in future. The effect of barrier pillars can also be simulated.

## 5 Conclusions

This paper is a case study of a large pillar collapse in the Everest Platinum Mine that led to the closure of this operation. A major contributing factor to the collapse was the presence of the so-called weak alteration layers in the pillars. From the literature survey, it is clear that weak seams in pillars reduce the strength and, in these situations, conventional pillar strength formulas overestimate the strength.

A novel numerical modelling approach is proposed in the paper to study the pillar failure and to conduct a back analysis of the mine collapse. This consisted of a limit equilibrium constitutive model implemented in a displacement discontinuity code. The model is an elegant method to introduce pillar failure in displacement discontinuity codes. It has a drawback, however, as it assumes a symmetrical model with partings with identical friction angles at both the hanging wall and footwall contacts of the pillar. This is,



therefore, only a first-order approximation of the “toppling” pillar failure mechanism at Everest Platinum Mine and a possible extension of the limit equilibrium model needs to be explored in future.

Different areas of the Everest Platinum Mine were simulated to conduct a preliminary calibration of the limit equilibrium model. These models illustrated that a reduction in friction angle on the partings, owing to the presence of water in the collapse area, seems to be a plausible factor that contributed to the collapse. Although encouraging results were obtained, calibration of the limit equilibrium model remains a challenge. Laboratory testing is required to determine the strengths of the weak partings and in particular, the difference in strength of the wet and dry alteration zone material needs to be established.

**Acknowledgements** This work forms part of the MSc study of the principal author, Paul Couto, at the University of Pretoria. The authors would like to thank Mr. Noel Fernandes for permission to use the historic data of the Everest Platinum Mine collapse.

## References

- Alejano LR, Arzua J, Castro-Filgueira U, Malan F (2017) Strapping of pillars with cables to enhance pillar stability. *J S Afr Inst Min Metall* 117:527–540
- Crouch SL, Starfield AM (1983) *Boundary element methods in solid mechanics*. George Allen and Unwin, London
- Deist FH, Georgiadis E, Moris JPE (1972) Computer applications in rock mechanics. *J S Afr Inst Min Metall* 72:265–272
- Deng S, Chen Y, Hou J, Feng J, Yang Y, Wu X (2018) Study on the influence of soil moisture content on the probability of landslide instability. In: 8th international conference on manufacturing science and engineering (ICMSE 2018), pp 532–536
- Du Plessis M, Malan DF, Napier JAL (2011) Evaluation of a limit equilibrium model to simulate crush pillar behavior. *J S Afr Inst Min Metall* 111:875–885
- Eriksson PG, Hattingh PJ, Altermann W (1995) An overview of the geology of the Transvaal Sequence and Bushveld Complex South Africa. *Miner Depos* 30(2):98–111
- Esterhuizen GS, Dolinar DR, Ellenberger JL (2011) Pillar strength in underground stone mines in the United States. *Int J Rock Mech Min Sci* 48:42–50
- Esterhuizen GS, Tyrna PL, Murphy MM (2019) A case study of the collapse of slender pillars affected by through-going discontinuities at a limestone mine in Pennsylvania. *Rock Mech Rock Eng* 52:4941–4952
- Esterhuizen GS, Ellenberger JL (2007) Effects of weak bands on pillar stability in stone mines: field observations and numerical model assessment. In: *Proceedings of 26th international conference on ground control in mining*. Morgantown, West Virginia, pp 320–326
- Gonzalez-Nicieza C, Alvarez-Fernandez M, Menendez-Diaz A (2006) A comparative analysis of pillar design methods and its application to marble mines. *Rock Mech Rock Eng* 39:421–444
- Hartzenberg AG, Du Plessis M, Malan DF (2019) The effect of alteration layers on UG2 pillar behaviour in the Bushveld Complex. In: *Proceedings 14th ISRM Congress, Foz do Iquacu, Brazil, 13–18 Sept 2019*
- Heasley KA (1998) Numerical modeling of coal mines with a laminated displacement-discontinuity code. PhD Dissertation, Colorado School of Mines
- Hedley DGF, Grant F (1972) Stope-and-pillar design for Elliot Lake uranium mines. *Bull Can Inst Min Metall* 65:37–44
- Lunder PJ, Pakalnis R (1997) Determination of the strength of hard rock mine pillars. *Bull Can Inst Min Metall* 68:55–67
- Malan DF, Napier JAL (2011) The design of stable pillars in the Bushveld mines: a problem solved? *J S Afr Inst Min Metall* 111:821–836
- Martin CD, Maybee WG (2000) The strength of hard-rock pillars. *Int J Rock Mech Min Sci* 37:1239–1246
- Napier JAL, Malan DF (2007) The computational analysis of shallow depth tabular mining problems. *J S Afr Inst Min Metall* 107:725–742
- Napier JAL, Malan DF (2018) Simulation of tabular mine face advance rates using a simplified fracture zone model. *Int J Rock Mech Min Sci* 109:105–114
- Napier JAL, Malan DF (2021) A limit equilibrium model of tabular mine pillar failure. *Rock Mech Rock Eng* 54:71–89
- Plewman RP, Deist FH, Ortlepp WD (1969) The development and application of a digital computer method for the solution of strata control problems. *J S Afr Inst Min Metall* 70:33–44
- Roberts MKC, Clark-Mostert V (2010) Is there some commonality between the geological structures in the Bushveld Complex and the Great Dyke? In: *The 4th international platinum conference, platinum in transition ‘Boom or Bust’*. S Afr Inst Min Metall, pp 149–155
- Ryder JA, Napier JAL (1985) Error analysis and design of a large-scale tabular mining stress analyser. In: *5th international conference on numerical methods in geomechanics, Nagoya, Japan, pp 1549–1555*
- Salamon MDG (1964) Elastic analysis of displacements and stresses induced by mining of seam or reef deposits—II. Practical methods of determining displacements, strain and stress components from a given mining geometry. *J S Afr Inst Min Metall* 64:197–218
- Stacey TR, Page CH (1986) *Practical handbook for underground rock mechanics*. Series on rock and soil mechanics, vol 12. Trans Tech Publications, Clausthal-Zellerfeld, Germany, pp 53–63
- Wyllie DC, Norrish, NI (1996) *Rock strength properties and their measurement. Landslides: Investigation and mitigation*. Transportation Research Board Special Report, Washington, no. 247, pp 372–390

**Publisher's Note** Springer Nature remains neutral with regard to jurisdictional claims in published maps and institutional affiliations.

Springer Nature or its licensor holds exclusive rights to this article under a publishing agreement with the author(s) or other rightsholder(s); author self-archiving of the accepted manuscript version of this article is solely governed by the terms of such publishing agreement and applicable law.